Double crosslinked biomimetic composite hydrogels containing topographical cues and WAY-316606 induce neural tissue regeneration and functional recovery after spinal cord injury

Xingchang Zhao [a,b,1], Xianzhe Lu [a,1], Kai Li [c,1], Shiqiang Song [a,1], Zhaohui Luo [d], Chuanchuan Zheng [a], Chengliang Yang [a], Xiumei Wang [f], Liqiang Wang [g], Yujin Tang [a,b,**], Chong Wang [e,***], Jia Liu [a,b,*]

[a] Department of Orthopaedics, Affiliated Hospital of Youjiang Medical University for Nationalities, Baise, Guangxi, China
[b] Guangxi Key Laboratory of Basic and Translational Research of Bone and Joint Degenerative Diseases, Guangxi Biomedical Materials Engineering Research Center for Bone and Joint Degenerative Diseases, Baise, Guangxi, China
[c] Academy of Orthopedics, Guangdong Province, Guangdong Provincial Key Laboratory of Bone and Joint Degeneration Diseases, The Third Affiliated Hospital of Southern Medical University, Guangzhou, China
[d] Youjiang Medical University for Nationalities, Baise, Guangxi, China
[e] School of Mechanical Engineering, Dongguan University of Technology, Songshan Lake, Dongguan, Guangdong, China
[f] State Key Laboratory of New Ceramics and Fine Processing, Key Laboratory of Advanced Materials of Ministry of Education, School of Materials Science and Engineering, Tsinghua University, Beijing, China
[g] State Key Laboratory of Metal Matrix Composites, School of Material Science and Engineering, Shanghai Jiao Tong University, Shanghai, China

ARTICLE INFO

ABSTRACT

Spinal cord injury (SCI) is an overwhelming and incurable disabling condition, for which increasing forms of multifunctional biomaterials are being tested, but with limited progression. The promising material should be able to fill SCI-induced cavities and direct the growth of new neurons, with effective drug loading to improve the local micro-organism environment and promote neural tissue regeneration. In this study, a double crosslinked biomimetic composite hydrogel comprised of acellularized spinal cord matrix (ASCM) and gelatin-acrylated-β-cyclodextrin-polyethene glycol diacrylate (designated G-CD-PEGDA) hydrogel, loaded with WAY-316606 to activate canonical Wnt/β-catenin signaling, and reinforced by a bundle of three-dimensionally printed aligned polycaprolactone (PCL) microfibers, was constructed. The G-CD-PEGDA component endowed the composite hydrogel with a dynamic structure with a self-healing capability which enabled cell migration, while the ASCM component promoted neural cell affinity and proliferation. The diffusion of WAY-316606 could recruit endogenous neural stem cells and improve neuronal differentiation. The aligned PCL microfibers guided neurite elongation in the longitudinal direction. Animal behavior studies further showed that the composite hydrogel could significantly recover the motor function of rats after SCI. This study provides a proficient approach to produce a multifunctional system with desirable physiological, chemical, and topographical cues for treating patients with SCI.

1. Introduction

Spinal cord injury (SCI) is a highly disabling condition. Once the spinal cord is directly or indirectly injured, a series of symptoms of sensory and motor dysfunction below the level of the SCI will be manifested [1]. Following SCI, spinal cord tissue ischemia, hypoxia, edema,

---

excessive release of lysosomal contents, infiltration of inflammatory factors, and initiation of autophagy will all cause changes in the microenvironment, resulting in neuronal degeneration and necrosis in a relatively short period [2,3]. This necrotic tissue is subsequently absorbed and liquefied to form a fluid-filled cyst. The formation of voids can diminish cytokine infiltration and axonal ingrowth, making it difficult for synapses to recover and eventually causing neurological dysfunction [4]. Strategies such as transplantation of neural stem cells (NSCs), inhibition of inflammatory factors, stimulation of neuronal differentiation, and promotion of nerve growth have certain therapeutic effects on SCI. However, a single therapeutic strategy has limited efficacy, because SCI is a complex pathological process [5]. Therefore, there is an urgent need to develop a multifunctional therapeutic strategy with greater efficacy.

The rapid development of biomaterials and tissue engineering provides us with opportunities to treat SCI more effectively. Biomaterials used for treating SCI have shifted from monolithic materials to biomimetic composite materials. For example, electrospun collagen/polycaprolactone (PCL) composite hydrogel scaffolds displayed both excellent mechanical strength and cellular affinity [6]. In our previous study, a decellularized spinal cord scaffold loaded with umbilical cord mesenchymal stem cells bridged the cavity caused by SCI and promoted long-distance axon regeneration and motor function recovery [7]. It is known that topographical features provided by the scaffolds play a crucial role in determining the cellular responses. Given that the direction of neurite outgrowth can be affected by nano-to micro-scale structural features, providing biomaterials with appropriate topographical guidance can accelerate neurite extension together with the axial direction of the spinal cord, thereby leading to a more rapid synapse connection.

Furthermore, the addition of functional drugs/biomolecules in scaffolds could elicit favorable cellular responses. In our previous study, spinal cord defects were filled with a decellularized scaffold containing bpv (Pic)-loaded polylactic acid microspheres, which activated mammalian target of rapamycin1 signaling by inhibiting gene of phosphate and tension homology deleted on chromosome ten through bpv (Pic) to enhance autophagy and inhibited cell apoptosis levels, thereby promoting neuronal repair and reducing neuronal loss [8]. Therefore, the optimized combination of certain biomaterials with drugs could be used as a desirable strategy for treating SCI.

The canonical Wnt/β-catenin signaling pathway is an essential signaling cascade that plays a key role in the regulation of neuronal differentiation, axonal extension, cell proliferation, and neuronal survival [9–11]. Several studies have reported that the activation of Wnt/β-catenin signaling after SCI promotes neuronal differentiation, axonal regeneration, and functional recovery [12–15]. Therefore, the targeted use of drugs to activate Wnt/β-catenin signaling may provide a novel approach for the recovery of spinal cord function in SCI. WAY-316606, a small molecular inhibitor of secreted frizzled-related protein (sFRP-1) [16,17], promoted bone formation in mice and inhibited apoptosis in human glioblastoma cells by activating canonical Wnt/β-catenin signaling [18,19]. However, the function of WAY-316606 has not been discussed in neuron regeneration and functional recovery in SCI.

In this study, a composite hydrogel was fabricated by combining three-dimensionally (3D) printed oriented PCL microfiber bundles produced through near-field direct write electrospinning with WAY-316606-loaded biomimetic hydrogels comprised of acellular spinal cord matrix (designated as ASCM) and gelatin-acrylated-β-cyclodextrin-polyethylene glycol diacrylate (designated as G-CD-PEGDA) hydrogels, to guide the growth of nerve axons, improve the microenvironment, and inhibit glial scar formation. The implantation of our WAY-316606-loaded composite hydrogel into the hemi-sectioned SCI rat model effectively recruited endogenous NSCs and allowed them to migrate to the lesion area, showing up-regulated neuronal differentiation together with the aligned PCL fibers and inhibited astrocyte differentiation. The

WAY-316606-loaded composite hydrogel scaffolds activated Wnt/β-catenin signaling to promote NSC differentiation and nerve cell growth, thereby repairing injured spinal cord tissue. Moreover, the motor function of rats with SCI was significantly improved. Overall, the 3D printed oriented PCL microfiber-reinforced WAY-316606-loaded composite hydrogel can be used as a suitable system to treat SCI.

2. Experimental

2.1. Preparation of 3D printed oriented PCL microfibers

Three-dimensionally printed oriented microfibers were prepared using the melt near-field direct writing electrospinning technology. First, after preheating the 3D printing near-field electrospinning machine (Foshan Lepton Precision Measurement And Control Technology Co., Ltd., Foshan, China), the polymer material PCL particles (Sigma, St. Louis, MO, USA) were placed into a clean stainless steel needle, which was put into the machine and inserted into the trachea and fixed. Subsequently, the heating device was turned on and the heating target temperature was set to 97 °C to heat for 20 min, and a 40 × 40 mm glass piece cleaned with alcohol was placed on the conductive glass plate. Finally, the pre-drawn computer program path (the X/Y/Z three-axis mapping, orientation arrangement, starting and ending points, etc.) was imported into the printer software, which was set with the following parameters: height 5 mm, speed 40 mm/s, acceleration 300 mm/s^2, preprocessing 1000 times, turning time 1000 ms, stacking layers 20, voltage 4.63 KV, and air pressure 4.98 KPa. The melted PCL was extruded from the tip of the nozzle under constant air pressure, stretched, and refined under the combined action of gravity, platform traction, and electric field (conductive glass applies high-voltage static electricity), and the extruded filaments were cooled and solidified to form microfiber deposits on a conductive glass substrate.

2.2. Preparation of rat acellularized spinal cord (ASC)

Ten two-month-old Sprague-Dawley rats (Tianqin Biotechnology Co., Ltd., Changsha, China) weighing approximately 200 g were euthanized with 3% pentobarbital sodium (4 ml/kg) by intraperitoneal injection of overdose anesthesia. The spinal cord was completely removed from the spinal canal. ASC was prepared by ice-melting and chemical extraction methods. The basic process was to remove the spinal cord and cool it for 2 h at −80 °C. Subsequently, it was placed at room temperature for rapid thawing. Finally, the spinal cord was repeatedly rinsed with ultra-pure (UP) water, 1%TritonX-100 (Sigma), and 1% sodium deoxycholate (Sigma) solution with oscillation. The cells were removed and the extracellular matrix (ECM) was retained, as described in our previous study [20]. The rinsed spinal cord specimens were placed in a freeze-drying machine (Christ, Osterode, Germany) and freeze-dried for 24 h. The spinal cord was opalescent, soft, light, and tough, and was stored at −80 for future use.

2.3. Preparation of drug-loaded ASC hydrogels

The shredded ASC scaffold was placed into 1.5 ml UP water, fully shaken and mixed to dissolve, filtered to remove undissolved substances, and finally, a milky white ASCM was formed. A total of 10 mg of the drug WAY-316606 (MCE, New Jersey, USA) was dissolved in 2229.8 μl dimethyl sulfoxide to a concentration of 10 mmol and diluted to a final working concentration of 2 μmol/L. A total of 1117 μl working solution (drug dose of 10 μg) was added to the ASCM to form a WAY-316606-loaded ASCM.

The components of the drug-loaded ASC hydrogel included gelatin 0.16 g, methacrylated β-cyclodextrin (AC-β-CD) 0.16 g, polyethylene glycol diacrylate (PEGDA) 0.05 g, photoinitiator phenyl (2,4,6-trimethyl benzoyl) phosphate lithium salt (LAP) 0.003 g, and WAY-316606-loaded ASCM. As each component was added to the WAY-316606-loaded

ASCM, the mixture was incubated in a 50 °C water bath, and then removed again each time to add the next component, finally forming the WAY-316606-loaded ASC hydrogel. The hydrogel was irradiated with ultraviolet light (UV) at 300–400 nm for 10 min to form a double-cross-linked WAY-316606-loaded ASC hydrogel [21], which was not yet solidified.

2.4. Preparation of 3D printed oriented microfiber-loaded WAY-316606/ASC hydrogel composite hydrogel scaffolds

The WAY-316606-loaded ASC hydrogel was filled on the 3D printed oriented microfibers, which were curled and shaped into a cylindrical shape similar to the spinal cord, placed in a confined space, and cured using 300–400 nm UV light for 10 min, and finally formed into a 3D printed oriented microfiber loaded WAY-316606/ASC hydrogel composite scaffold. The composite scaffold was freeze-dried for 24 h, sterilized using gamma-ray irradiation, and stored at −80 °C for future use.

2.5. In vitro degradation assay of scaffolds

Scaffold residual weight (%) was used to investigate scaffold degradation in vitro over 8 weeks. The weighed samples were immersed in centrifuge tubes containing phosphate-buffered saline (PBS, pH 7.4, containing 1% penicillin-streptomycin mixture). The centrifuge tube was sealed with parafilm and placed in a constant temperature shaker (temperature 37 °C, speed 30 rpm), and the PBS solution was replaced every 3 days. At each time point (2, 4, 6, and 8 weeks), three samples were taken from the test tube for each group, placed in a freeze dryer to dry for 48 h, and weighed. The percentage of the remaining weight and the initial weight were used to determine the degradation rate.

2.6. Physicochemical characteristics of composite hydrogel scaffolds

A standard light microscope was used to observe the arrangement, diameter, and wire drawing of the 3D printed oriented fibers. The macroscopic and microscopic morphologies of the composite hydrogel scaffolds were observed using a smartphone camera (Huawei HONOR30, China) and a scanning electron microscope (Leo 1530 Gemini, Zeiss, Oberkochen, Germany), respectively. The lyophilized samples were coated with a thin layer of gold and the microscopic morphology of the composite hydrogel scaffolds was observed from longitudinal and transverse sections. By testing five samples, the orientation of the 3D printed oriented fibers, the structure of the composite hydrogel, and the relationship between the oriented fibers and the composite hydrogel were studied.

2.7. In vitro biocompatibility evaluation

Rat NSCs and complete medium and differentiation medium kits were purchased from OriCell Company (Guangzhou, China). The main components of the complete medium set were OriCell SD rat neural stem cell basal medium 96 ml, B27 supplement 2 ml, penicillin-streptomycin 1 ml, L-glutamine 1 ml, heparin 0.1 ml, basic fibroblast growth factor 0.02 ml, and epidermal growth factor 0.01 ml. The main components of the differentiation medium kit were neural stem cell neurogenic differentiation basal medium 97 ml, neural stem cell neurogenic differentiation supplement 2 ml, and glutamax 1 ml. First, the NSCs were cultured in a complete medium for 3 days, the cells were collected and centrifuged for 4 min at 160 *g*, then resuspended in a differentiation medium, and co-cultured with composite hydrogel scaffolds (divided into two groups; one group was drug-free composite hydrogel scaffolds, one group was WAY-316606-loaded composite hydrogel scaffolds) to make the cells grow adherently. NSCs were cultured on the first and third days for cell activity detection, live/dead cell staining, and cell counting to evaluate the biocompatibility and cytotoxicity of the composite hydrogel scaffolds. The general process of staining was as follows:

First, the medium in the well of the culture plate was aspirated and the cells were washed twice with sterile PBS solution for 2 min each time. Subsequently, 500 μl calcein-AM and PI mixed dyeing solution (Dong-Ren Chemical Technology Co., Ltd., Shanghai, China) was added to each well of the 24-well laser confocal special culture plate (Hangzhou Xinyou Biotechnology Co., LTD. Hangzhou, China), which was placed in a CO_2 incubator at 37 °C under 5% CO_2 and saturated humidity for 30 min. After the dyeing was completed, the mixed dyeing working solution was aspirated, the cells were washed twice with sterile PBS solution for 3 min each time, and finally, 500 μl complete medium was added to each well of the 24-well plate. Cells were observed using a confocal laser scanning microscope, simultaneously observing live cells with yellow-green fluorescence and dead cells with red fluorescence at an excitation wavelength of 490 nm.

2.8. Immunofluorescence staining and imaging

Cells used in the vitro experiments were divided into three groups: Control group (medium only), Scaffold group (medium + drug-free composite hydrogel scaffold), and WAY-316606 + Scaffold group (medium + WAY-316606-loaded composite hydrogel scaffold). Cells were fixed with 4% paraformaldehyde (Biosharp, Hefei, China) for 20 min, whereas the spinal cord was not fixed with paraformaldehyde. Following washing with PBS, the cells or tissues were blocked with 10% goat serum for 1 h, washed three times for 5 min with PBS, incubated with primary antibody for 12 h at 4 °C and washed three times for 5 min in PBS. The cells or tissues were subsequently incubated with the corresponding secondary antibody at room temperature for 1 h and washed three times for 5 min in PBS. Finally, 2-(4-)-6-indolecarbamidine dihydrochloride (Sigma) staining was performed. A cover glass was used to seal the spinal cord tissue. Confocal images were obtained using a Leica LSM 800 confocal microscope (Leica, Wetzlar, Germany).

2.9. Ethics statement

All the animal experimental protocols were approved by the Animal Ethics Committee of Youjiang Medical University for Nationalities, and the experimental animals were used according to the requirements of the Animal Welfare Ethics Committee.

2.10. Animals and SCI surgery

Adult female Sprague-Dawley rats (Tianqin Biotechnology Co., Ltd., Changsha, China) (230–250 g, n = 32) were randomly assigned to four groups: the sham-operated group (Sham, n = 8), spinal cord only half-cut group (SCI, n = 8), drug-free scaffold group (Scaffold, n = 8), and WAY-316606 + Scaffold group (WAY-316606 + Scaffold, n = 8). The rats were anesthetized by intraperitoneal injection of 3% sodium pentobarbital (1 ml/kg). Following successful anesthesia, the animal was fixed on the animal operating table in a prone position, the lamina was removed, and the thoracic 10 spinal cord was exposed, as previously reported [8]. Subsequently, an iris knife was used to excise the spinal cord with a length of approximately 0.2 cm on the right side to form a cavity. During this intervention, the rats were observed shaking violently and tail-waving, indicating that the modeling was successful. The scaffolds were cut to a length of approximately 0.2 cm and implanted into the defect area following immersion in PBS for 30 min. The incision was completely hemostatic, and the muscle layer, deep fascia, subcutaneous, and skin were sutured layer by layer. Following the operation, the rats were placed in a rewarming box until they awakened. The rats were intramuscularly injected with penicillin for 3 days and bladder massaged to urinate twice daily until normal urination was restored.

2.11. Recovery and analysis of motor function

The motor function recovery of the hind limbs Basso-Beattie-Bresnahan (BBB) motor function score of the rats was observed weekly after the operation, and the observation was performed for 8 weeks in total. Animals were observed in an open area for 5 min, followed by BBB scoring. To evaluate the body balance and lower limb muscle strength of the rats, a 45-degree slope grid test was performed at 8 weeks after the operation. During the test, a wire mesh with a mesh diameter of 1 cm was placed at a 45-degree angle, and the rat was placed on it to observe the animal's crawling posture and foot position.

2.12. Histological staining

Eight weeks after the operation, the rats were anesthetized by intraperitoneal injection of 3% sodium pentobarbital (/kg). Following successful anesthesia, the rats underwent intracardiac perfusion with 200 ml 0.9% normal saline followed by 250 ml 4% paraformaldehyde. As the rats were perfused with paraformaldehyde, severe muscle tremors and tail "dancing" were observed in these animals, indicating that the heart was perfused successfully. The spinal cord was removed and fixed in 4% paraformaldehyde for 24 h. The SCI segment was cut to a length of 2 cm. Spinal cords were dehydrated in a gradient of 15% and 30% sucrose, embedded in optimal cutting temperature compound, and frozen in longitudinal and transverse sections (thickness 12 μm). The samples were stained with hematoxylin-eosin (HE) and Nissl, and images were acquired with an Olympus upright microscope.

2.13. Statistical analysis

Data were analyzed using SPSS v16.0 (IBM, USA). Measurement data were expressed as mean ± standard deviation (SD). Data were analyzed using a nonparametric one-sample Kolmogorov-Smirnov Test or one-way analysis of variance (ANOVA) with Homogeneity of variance test. Multiple comparisons between groups were performed using one-way ANOVA with least significance difference and Student Newman Keul's post-hoc test. Tamhane's T2 was used if equal variances were not assumed. Error bars represent SD. $P < 0.05$ statistical significance.

3. Results and discussion

3.1. Design and characterization of PCL microfibers/ASCM/G-CD-PEGDA composite hydrogel scaffolds

Fig. 1 shows the schematic of making PCL microfiber-reinforced WAY-316606 composite hydrogel scaffold and implantation of the composite hydrogel scaffolds into the SCI tissue defects. Near-field direct writing electrospinning technology has gained attention in the fields of biology and tissue engineering and has been widely used in tissue engineering scaffolds [22–24]. Through the near-field direct writing electrospinning technology, the diameter of the electrospun fibers and the gap between the spinning fibers can be controlled, and they can be stacked layer by layer [25–27]. The aligned PCL microfibers with desirable biocompatibility and mechanical property bridged both ends of the SCI region to provide topographical guidance for directional extension of axons and neurites, and hence reduce cell clustering and disorderly growth of neurites [13,28–30]. The ASCM, which contains a large number of polysaccharides, proteins, and signaling molecules [31, 32], can provide a favorable microenvironment for neural tissue regeneration and regulate the cellular behavior of NSCs [33]. The self-healable G-CD-PEGDA hydrogel with a dynamic double crosslink network can maintain its structural stability during the degradation process and provide a favorable space for endogenous NSC migration and neurite extension [6,34–36]. The drug WAY-316606, which is slowly released by the composite hydrogel scaffolds, can activate canonical Wnt/β-catenin signaling by inhibiting sFRP-1, thereby promoting nerve cell proliferation [37–39].

It can be seen from Fig. 2A and B that PCL microfibers made through the near-field direct write electrospinning were in a parallel arrangement with an average diameter of 19.17 ± 4.29 (Fig. 2B). Fig. 2C shows the macroscopic morphology of the ASC, which retains the ECM network. The ASC had a milky white color and a sponge-like state. The
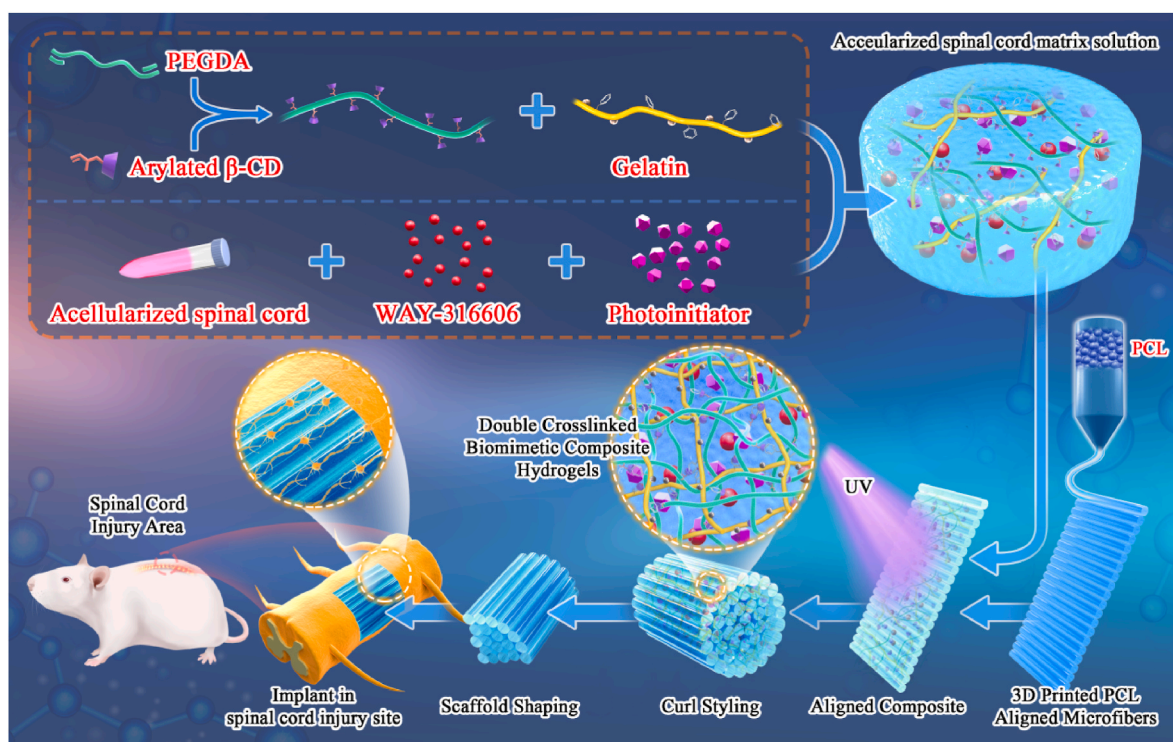

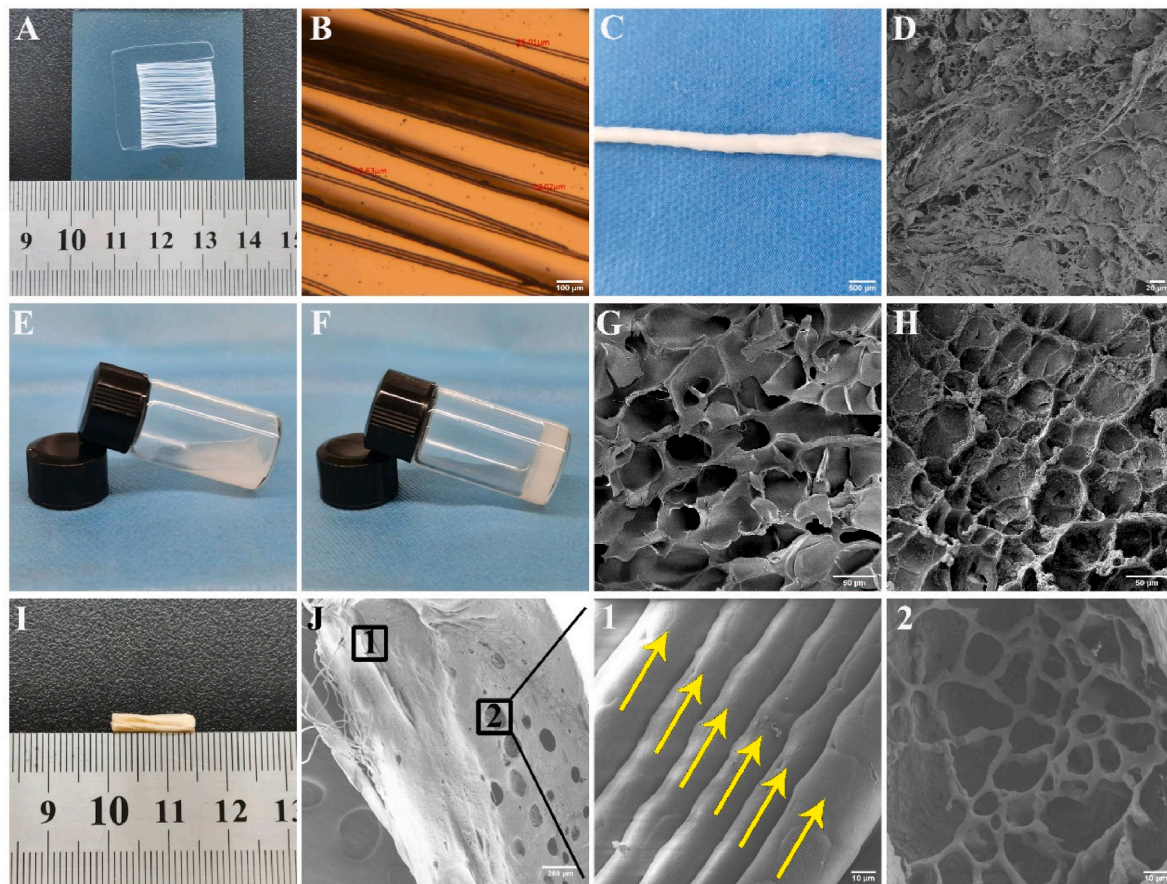**Fig. 1.** The preparation process of the composite component scaffold.

Fig. 2. Physicochemical properties of the composite hydrogel scaffolds and their components. A) The general view of 3D printed oriented PCL fibers shows that the fibers are oriented in a directional arrangement. B) Microscopic morphology of oriented fibers, the red number is the fiber diameter (scale bar 100 μm). C) The macroscopic view of the ASC after freeze-drying (scale bar 500 μm). D) SEM morphology of ASC, showing a porous network structure, which was intertwined (scale bar 20 μm). E, F) State of the ASCM-G-CD-PEGDA composite hydrogel before and after curing. Before curing, it is a flowable gel, and after curing, the viscosity increases and it can be adhered to the bottom of the bottle. G) SEM image of the ASCM-G-CD-PEGDA hydrogel (scale bar 20 μm). H) SEM image of the WAY-316606-loaded hydrogel (scale bar 10 μm). I) General view of the composite hydrogel scaffolds. J) SEM image of the composite hydrogel scaffolds (1 and 2 represent partially enlarged images with yellow arrows designating oriented fibers, and the scale is 10 μm).

scanning electron microscope (SEM) micrograph showed that the ASC had a 3D porous structure with randomly distributed ECM fibers that formed a network structure (Fig. 2D). Fig. 2E and F shows the state of the G-CD-PEGDA hydrogel before and after photo-crosslinking at 37 °C, in which complexation between the benzene ring in gelatin and the bowl-like structure of acrylated-β-CD occurred to form the first crosslinking network, while radical polymerization between PEGDA and acrylated-β-CD was initiated by the photoinitiator LAP and UV irradiation at 365 nm to form the second crosslinking network. The double crosslinking network endowed the hydrogel with a self-healing property. Fig. 2G and H shows the microstructure of the ASCM-G-CD-PEGDA and WAY-316606-loaded ASCM-G-CD-PEGDA hydrogels after freeze-drying treatment. A honeycomb-like porous structure, which could facilitate cell adhesion, proliferation, and migration [40], was obtained for both types of hydrogels, and drug aggregates (i.e., WAY-316606) were uniformly distributed in the honey comb porous structure. The incorporation of drugs in the hydrogel matrix could increase the stability of the drug and enable its release in a more sustained manner [41]. Fig. 2I and J shows the macroscopic and microscopic morphology, respectively, of PCL microfiber-reinforced WAY-316606-loaded ASCM/G-CD-PEGDA composite hydrogel. The composite hydrogel had a cylindrical shape, with a length of 15 mm and a diameter of 3 mm (Fig. 2I), in which aligned PCL microfiber bundles were wrapped with WAY-316606-loaded ASCM-G-CD-PEGDA hydrogel. The PCL fiber bundles were oriented uniformly, which enables cells to grow in one

direction along the oriented fibers while avoiding cells growing in clusters and losing direction during growth and migration (Fig. 2J).

3.2. In vitro degradation and biocompatibility of composite hydrogel scaffolds

Hydrolytic degradation of the scaffolds was evaluated over 8 weeks with a particular focus on weight loss. SEM micrographs showed that the PCL microfibers before and after 8 weeks of degradation were still oriented and encapsulated by the hydrogels; the hydrogels had a 3D porous structure and were cross-connected to each other (Fig. 3A), suggesting that the PCL microfiber bundle-reinforced double-crosslinked composite hydrogel has a stable structure and can maintain the pre-designed shape after 8 weeks of incubation. After 2, 4, 6, and 8 weeks of degradation, the composite hydrogel displayed 5.08%, 9.24%, 16.49%, and 22.53% weight loss, respectively (Fig. 3B).

Biocompatibility of the composite hydrogel was examined by live/dead cell staining. The viability of NSCs co-cultured with drug-free composite hydrogel scaffolds for 1 and 3 days were 81.45% ± 0.58% and 77.61% ± 4.26%, respectively, while NSC viability when co-cultured with the drug-loaded composite hydrogel scaffolds for these days were 84.14% ± 2.38% and 81.54% ± 2.17%, respectively (Fig. 3C), indicating that both the drug-free and the drug-loaded composite hydrogel scaffolds were biocompatible and there was no significant difference in the viable cell rate between the two groups. Confocal
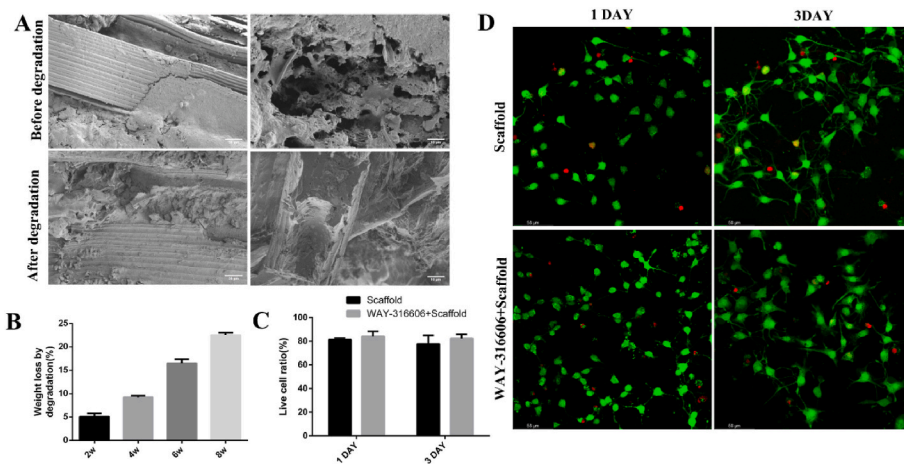
Fig. 3. Degradation rate and in vitro compatibility of composite hydrogel scaffolds. A) SEM images of composite hydrogel scaffolds before and after degradation. In the figure, a and b and c and d are the microscopic characterizations of the longitudinal section and cross-section of the composite hydrogel scaffolds before and after degradation, respectively; (scale bar: a, c are 50 μm; b, d are 10 μm). B) The degradation rates of composite hydrogel scaffolds at 2, 4, 6, and 8 weeks. C) The viable cell rates of NSCs co-cultured with the two different composite hydrogel scaffolds. D) CLSM micrographs of NSCs co-cultured with scaffolds for 1 and 3 days, with live cells in green and dead cells in red (scale bar 58 μm). (Error bars represent SD, n = 4).

laser electron microscopy (CLSM) micrographs showed that only a few dead NSCs (colored red) were observed in both the drug-free and drug-loaded composite hydrogel scaffolds (Fig. 3D). Biodegradability is one of the basic characteristics of tissue engineering materials [42,43]. The degradation speed of the material must meet the needs of cell growth.

3.3. Drug-loaded composite hydrogel scaffolds promote NSC neuronal differentiation and inhibit astrocyte differentiation

NSCs can differentiate into neurons, astrocytes, oligodendrocytes, and microglia among others. To observe the effect of the drug-loaded composite hydrogel scaffolds on NSC differentiation to astrocytes, drug-loaded composite hydrogel scaffolds were co-cultured with NSCs for 10 days. In total, 83.22% ± 2.15% and 68.15% ± 3.48% GFAP$^+$ cells were observed in the Control and WAY-316606 + Scaffold groups, respectively (P < 0.05, Fig. 4A and B), indicating that the drug-loaded composite hydrogel scaffolds can effectively inhibit differentiation along the astrocyte lineage. In addition, whether the neuronal cells differentiated from NSCs eventually differentiated to mature neuronal cells was determined by immunofluorescence for mature neuronal cell marker proteins microtubule-associated protein 2 (MAP2) and neuronal nuclei (NeuN) (Fig. 4C and D). Following 21 days of culture, 32.24% ± 0.79%, 40.02% ± 4.88%, and 63.37% ± 3.47% MAP2$^+$ cells were observed in the Control, Scaffold, and WAY-316606 + Scaffold groups, respectively. The Scaffold and WAY-316606 + Scaffold groups achieved significantly better neuron growth than the Control group (P < 0.01), in

which the value in the WAY-316606 + Scaffold group was significantly higher than that in the Scaffold group (P < 0.05); 31.5% ± 2.73%, 44.51% ± 5.48%, and 59.79% ± 2.99% NeuN$^+$ cells were observed in the Control, Scaffold, and WAY-316606 + Scaffold groups, respectively. The neuronal differentiation of NSCs and maturation of neurons in the Scaffold and WAY-316606 + Scaffold groups were significantly better than those in the Control group (P < 0.05); and the WAY-316606 + Scaffold group was better than the Scaffold group (P < 0.05). These data demonstrated that the composite hydrogel scaffolds can promote neuronal growth and provide a cellular basis for SCI repair. The difference between the Scaffold and WAY-316606 + Scaffold groups could be attributed to the effect of the drug WAY-316606 loaded on the composite hydrogel scaffold, suggesting that WAY-316606 can promote neuronal cell growth.

3.4. Composite hydrogel scaffolds promote NSC differentiation and growth by regulating the Wnt/β-catenin signaling pathway

Because WAY-316606 can indirectly activate the Wnt/β-catenin signaling pathway, whether the proteins of this signaling pathway are continuously expressed and whether their levels change during NSC differentiation should be elucidated. To investigate the role of Wnt/β-catenin signaling in NSC differentiation, the expression of β-catenin and downstream proteins of Wnt/β-catenin signaling (including transcription factor 4 (TCF4) and lymphoid enhancing factor (LEF1)) were examined during NSC differentiation. With the prolongation of the
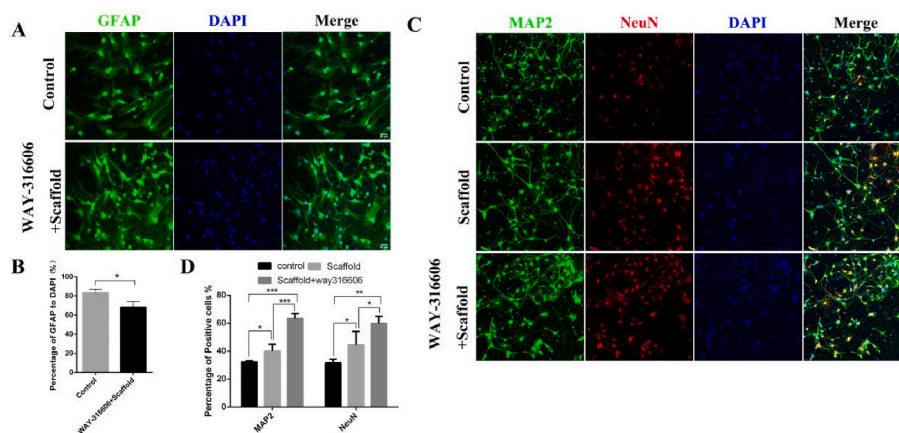

Fig. 4. Effect of 3D printed composite hydrogel scaffolds on NSC differentiation in vitro. A, B) WAY-316606-loaded composite hydrogel scaffolds inhibited the increase of GFAP (green). The Control and WAY-316606 + Scaffold composite hydrogel scaffold groups were quantitatively analyzed. C, D) Composite hydrogel scaffolds can promote neuronal cell differentiation. All data are presented as mean ± SD, n = 3. Scale: 50 μm *P < 0.05, **P < 0.01, ***P < 0.001.

differentiation induction time, the cell body became larger and the synapse became longer under the bright field of the inverted microscope. Immunofluorescence staining of NSCs showed that β-catenin protein was localized in the nucleus and cytoplasm, TCF4 protein was mainly localized in the nucleus, with less content in the cytoplasm, and LEF1 protein was localized in the nucleus, but not expressed in the cytoplasm (Fig. 5A). The expression of β-catenin, TCF4, and LEF1 was already detected on the first day of NSC differentiation. With the cell growth, the β-catenin protein content increased gradually. The mean fluorescence intensity of total β-catenin protein in nerve cells on days 1 (132.08 ± 4.86), 3 (167.57 ± 4.88), 5 (170.65 ± 2.91), 7 (192.87 ± 6.29), and 10 (203.10 ± 7.90) showed that the total β-catenin protein level in cells gradually increased with time (Fig. 5B). During the first 3 days after the induction of NSC differentiation, the up-regulation was the greatest, and then gradually increased at a slower rate. The total β-catenin protein content in cells was significantly different between day 1 and days 3, 5, 7, and 10 ($P < 0.01$). There were significant differences between the 3rd day and other days except the 5th day ($P < 0.01$). There were significant differences between the 7th day and other days except the 10th day ($P < 0.01$). Over the same time period, the β-catenin protein content in the nucleus was determined. From days 1–10, the β-catenin protein content in the nucleus gradually increased with time (Fig. 5C). Similar to the total β-catenin protein expression in the cells, the β-catenin protein content in the nucleus increased significantly over 1–3 days and 5–7 days. It is of note that the increase of β-catenin protein was slow over days 3–5 and 7–10, and there was a clear "plateau". Whether this phenomenon is associated with the protein synthesis cycle in the nucleus of nerve cells requires more in-depth research. The total intracellular TCF4 protein expression increased slightly with time from days 1–10, but there was no significant difference between the different days ($P > 0.05$, Fig. 5D). The TCF4 protein content in the nucleus was significantly different on the first day compared with the other days except for the third day, and was most significantly different on the tenth day ($P < 0.01$). Although there was an increasing trend on days 3, 5, and 7, there was no significant difference, while there was a significant difference between day 10 and all the rest of the days ($P < 0.01$, Fig. 5E). We performed immunofluorescence staining for LEF1 protein and found that there were significant differences between the first day of NSC differentiation and the other days ($P < 0.01$, Fig. 5F). The third day was significantly different from the other days except for the fifth day ($P < 0.01$). The staining gradually increased on days 5, 7, and 10, but this was not significantly different ($P > 0.05$). Therefore, we concluded that β-catenin, TCF4, and LEF1 accumulated in the nucleus during NSC differentiation, indicating that Wnt/β-catenin signaling is involved in the regulation of NSC differentiation.

Second, in this study, the 3D printed WAY-316606-loaded composite hydrogel scaffolds were co-cultured with NSCs, and we verified the effect of the drug-loaded composite hydrogel scaffolds on NSCs by detecting β-catenin and LEF1 protein expression. On the fifth day of induction of NSC differentiation, immunofluorescence staining for β-catenin and LEF1 proteins was performed (Fig. 5G). The total intracellular β-catenin protein content in the WAY-316606+Scaffold and WAY-316606 groups was significantly higher than that in the Control group (medium only) ($P < 0.05$) (Fig. 5H). The β-catenin protein content in the nucleus of the experimental group was significantly higher than that of the Control group ($P < 0.05$, Fig. 5I). At the same time, we determined the LEF1 protein expression in the nucleus, and there was a significant difference between the Control and experimental groups ($P < 0.05$, Fig. 5J). There was no difference in β-catenin and LEF1 protein between WAY-316606+ scaffold and WAY-316606 groups. These data indicated that the WAY-316606-loaded composite hydrogel scaffolds can upregulate β-catenin and LEF1 protein expression and activate Wnt/β-catenin signaling. The above experimental results showed that NSC differentiation and proliferation are closely associated with Wnt/β-catenin signaling. The 3D printed directional microfiber WAY-316606-loaded composite hydrogel scaffolds can activate the Wnt/β-catenin

signaling pathway, which can promote β-catenin protein accumulation in cells and its transfer to the nucleus, further up-regulating the expression of the downstream proteins TCF4 and LEF1, thereby promoting NSC differentiation and growth.

3.5. Drug-loaded composite hydrogel scaffolds regenerate defect spinal cord tissue and stimulate motor function recovery

Following SCI, tissue ischemia and hypoxia lead to secondary inflammation, apoptosis, and absorption of necrotic tissue to form a fluid cyst. Cavity formation will inhibit nerve axon ingrowth, eventually making it difficult to restore nerve function [4]. Therefore, filling the injured area with advanced biomaterials can reduce liquefaction and facilitate neural tissue regeneration. The composite hydrogel with a semicylinder shape (length: 2 mm; diameter: 1.5 mm) was implanted into the spinal cord with a semi-sectioned defect (length: 2 mm), and spinal cord regeneration was observed 2 and 8 weeks after the operation. In the Sham group, the surface of the spinal cord was smooth, the texture was uniform, and there was no obvious scar formation. In the SCI group, the spinal cord defect was obvious and the boundary was clear, and the defect area at 8 weeks was larger than that at 2 weeks. In the Scaffold and WAY-316606 + Scaffold groups, there was no obvious defect in the spinal cord, and the surface was smooth. In the WAY-316606 + Scaffold group, the tissue regeneration in the defect area was more complete than that in the Scaffold group, and the boundary line was more blurred and closer to normal spinal cord tissue (Fig. 6A). To further study the changes in microstructure and cavity area, longitudinal and transverse sections of the spinal cord were stained with an HE agent. In the Sham group, intertwined fibers were evenly distributed in the sectioned spinal cord, and there was no obvious cavity formation. There was no obvious tissue growth in the defect area in the SCI group, whereas the defect area in the WAY-316606 + Scaffold and Scaffold groups was well filled, and the directional fibers could connect both ends (Fig. 6B and C). The cavity area of the Scaffold groups (0.06 ± 0.006 mm^2) and WAY-316606 + Scaffold (0.05 ± 0.006 mm^2) was significantly smaller than that of the SCI group (0.37 ± 0.08 mm^2) ($P < 0.05$, Fig. 6D). Of note, directional microfibers were observed from both longitudinal and transverse sections of the groups implanted with composite hydrogel, and the PCL fibers were surrounded by tissue, which provided a topographical cue to guide heterogeneous neural tissue regeneration. Moreover, Nissl staining showed that the number of Nissl bodies in the WAY-316606 + Scaffold (50.5 ± 1.9/mm^2) and Scaffold groups (35.8 ± 1.1/mm^2) were significantly higher than those in the SCI group (6.0 ± 0.4/mm^2) ($P < 0.05$), and they were all distributed around the fibers (Fig. 6E). The pathological regeneration of spinal cord tissue suggested that the composite hydrogel could promote tissue regeneration.

To evaluate the motor function recovery in rats implanted with composite hydrogel, the left lower limb paralysis model was generated after hemisection of the spinal cord. Following implantation, the BBB motor function score was determined weekly, the scores being made by two observers numerous times to avoid possible errors. At 8 weeks after surgery, the BBB scores of the WAY-316606 + Scaffold (18.4 ± 0.5) and Scaffold groups (16.5 ± 0.7) were significantly higher than those of the SCI group (12.4 ± 0.3) ($P < 0.05$), with the WAY-316606 + Scaffold group significantly higher than the Scaffold group (Fig. 6F). In the process of exercise recovery, each group displayed the greatest improvement in exercise during the first 4 weeks and subsequently entered a plateau phase. To observe the joint movement, grip strength and body balance of the left lower limb, a grid test was performed (Fig. 6G). Rats in the Sham group had strong lower limbs, which supported the body to balance and crawl upwards, and thus the animals moved rapidly. In the SCI group, the muscles of the left lower limb were atrophied, and the left lower limb could not support the left body when crawling upward, resulting in drag. Animals of both the WAY-316606 + Scaffold and Scaffold groups could crawl up with the left lower limb
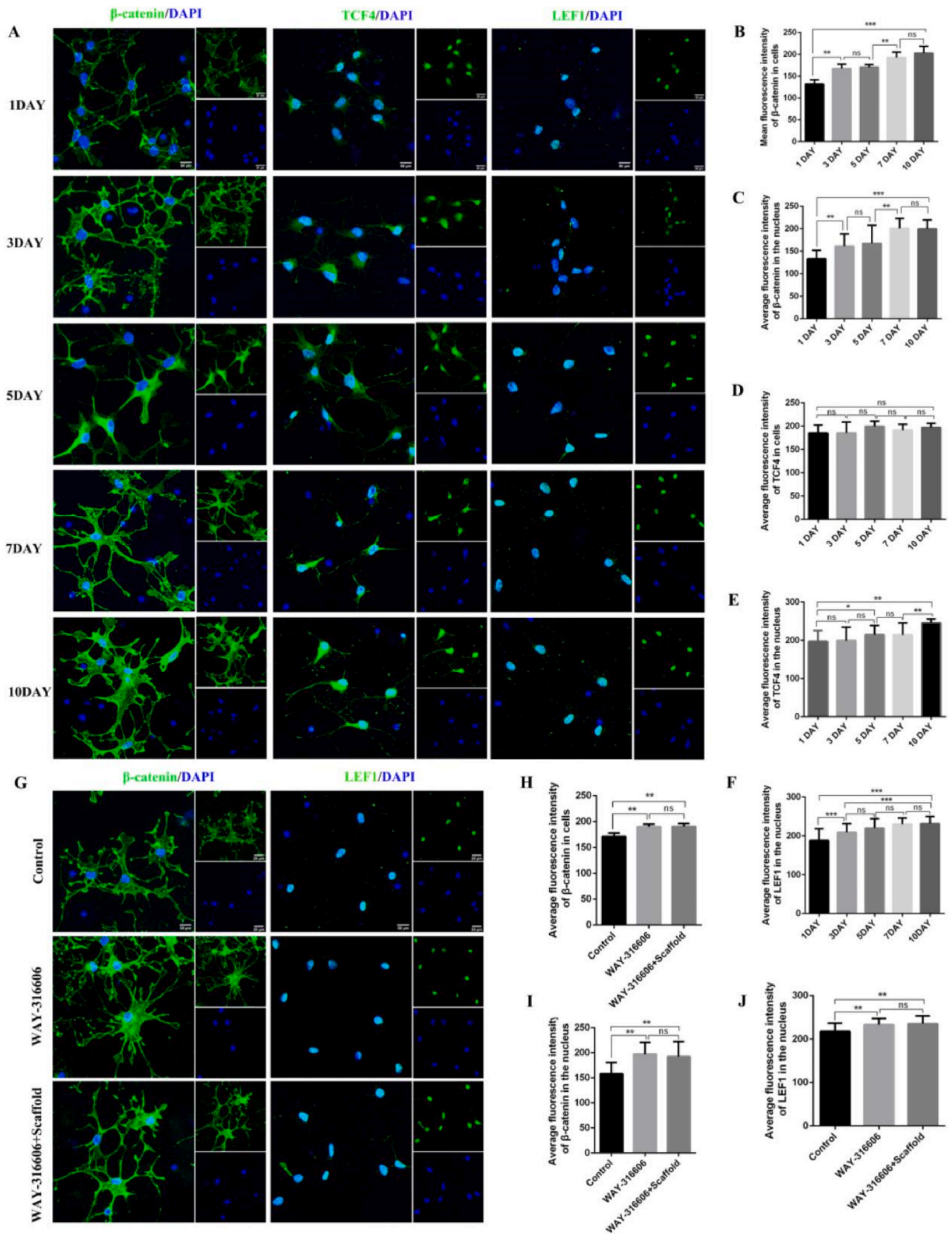
(caption on next page)

Fig. 5. Three-dimensionally printed WAY-316606-loaded composite hydrogel scaffolds activate Wnt/β-catenin signaling to promote NSC differentiation and growth. A) Expression of β-catenin (green), TCF4 (green), and LEF1 (green) proteins during NSC differentiation. B) Expression of the total β-catenin protein in neurons on different days. C) Expression of the β-catenin protein in the nucleus of neurons on different days. β-catenin protein expression was up-regulated from days 1–10. D) Total TCF4 protein expression in neural cells. E) TCF4 protein expression in the nucleus of nerve cells. F) Mean fluorescence intensity of LEF1 protein expression in the nucleus of nerve cells. G) The WAY-316606-loaded composite hydrogel scaffolds were co-cultured with NSCs for 5 days. H) Expression of the total β-catenin protein in neurons. I) Expression of the β-catenin protein in the nucleus of nerve cells. J) LEF1 protein expression in the nucleus of neurons. Note: The large icon ruler on the left side of Figs. A and D: 50 μm, and the small icon ruler: 20 μm. The size of the image is 40 ×, Zoom: 2.0. *P < 0.05, **P < 0.01, ***P < 0.001. ns means no significance.

supporting the body, and the melon could hold the grid. The coordination of the upper and lower limbs was poorer than that of the Sham group. These results indicated that the composite hydrogel can enhance the regeneration capability after SCI, and promote the recovery of nerve and motor function through the ingrowth of nerve cells.

3.6. Three-dimensionally printed composite hydrogel scaffolds recruited endogenous NSCs to migrate to the lesion area and induced their differentiation into neural lineage cells

To further study the effect of composite hydrogel scaffolds on SCI repair and to elucidate local nerve regeneration and glial scarring in the lesion site, the effect of composite hydrogel scaffolds on endogenous NSCs was investigated. Neuronal regeneration includes migration, proliferation, and neuronal differentiation of endogenous NSCs. Nestin is a marker protein of endogenous NSCs. NSCs were observed to be mostly distributed in the central canal and parenchyma of the spinal cord in its longitudinal section. In the composite scaffold groups (Scaffold group and WAY-316606 + Scaffold group), a large number of Nestin+ cells were observed in the lesion site, were distributed along the 3D printed directional fibers, and were connected to the two ends of the defect area. By comparison, in the spinal cord defect in the SCI group, Nestin+ cells were relatively rare. These results suggested that the composite scaffold could recruit endogenous NSCs and drive them to migrate to the injury site (Fig. 7A). Another key question is whether migrated endogenous NSCs can differentiate into neuronal cells. By immunofluorescence staining for Tuj1 and GFAP, Tuj1+ and GFAP+ cells were detected in the lesion site and marginal areas in the SCI, Scaffold, and WAY-316606 + Scaffold groups. (Fig. 7B). A large number of Tuj1+ cells were observed in and near the lesions of the Scaffold and WAY-316606 + Scaffold groups, which were considered to be derived from endogenous NSC differentiation, whereas many fewer such cells were observed in the SCI group. By contrast, in the SCI group, excessive reactive astrocytes aggregated in and around the lesion site to form a glial scar, which further inhibited NSC migration and neurite outgrowth. In the local enlarged image, it can be observed that Tuj1 and GFAP are expressed both in and around the lesion, indicating that the composite hydrogel scaffolds can recruit endogenous NSCs and induce them to differentiate into neural cells. In addition, we quantified the Tuj1 and GFAP expression levels according to their corresponding positive staining area percentages. The GFAP expression level around the lesion in the SCI group (18.70% ± 1.43%) was significantly higher (P < 0.01) than that in the Scaffold (10.62% ± 2.98%) and WAY-316606 + Scaffold groups (7.19% ± 1.26%) (Fig. 7C), and the level of the lesion (16.75 ± 2.14%) was also higher than the Scaffold (11.28 ± 1.10%) and WAY-316606 + Scaffold groups (6.02% ± 0.91%) (Fig. 7D). The Tuj1 level was the opposite to that of GFAP, and the WAY-316606 + Scaffold group was significantly higher than the Scaffold and SCI groups at the lesion site and edge (Fig. 7E and F). The results showed that the composite hydrogel scaffolds had a significant regenerative effect, and the WAY-316606-loaded composite hydrogel scaffolds had the greatest effect. These results suggested that the 3D printed composite hydrogel scaffolds can recruit endogenous NSCs to migrate to the lesion area and induce neural lineage cell differentiation, promote nerve regeneration, and reduce glial scar formation.

3.7. Three-dimensionally printed composite hydrogel scaffolds reduced neuroinflammation and promoted motor neuron differentiation

To investigate the immune response of spinal cord tissues to the composite hydrogel scaffolds, the expression of a marker protein of microglia, ion calcium-binding adapter molecule 1 (IBA1), was investigated. IBA1 is associated with acute neuroinflammation in central nervous system injury or exogenous implantation [44]. As shown in Fig. 8, microglia (IBA1+) were observed in the lesion and adjacent tissues in all groups 2 weeks after the operation. The number of IBA1+ cells in the SCI group (257.50 ± 24.75/mm²) was significantly higher than in the Scaffold (216.75 ± 6.18/mm²) and WAY-316606 + Scaffold groups (186.75 ± 4.92/mm²) at the lesion site and its adjacent regions, while the number in the Sham group was only 87.75 ± 6.40/mm² (Fig. 8A, C). These observations suggested that the composite hydrogel reduced the inflammatory response around the SCI region. The composite hydrogel scaffolds not only improved tissue regeneration but also promoted the number of HB9 and synaptophysin (SYN), by showing significantly higher HB9 and SYN expression levels in the Scaffold and WAY-316606 + Scaffold groups than in the SCI group (Fig. 8A, D, and E). Of note, the composite hydrogel scaffolds with directional topographical cues guided the neural tissue regeneration in the lesion site. Motor nerves and SYNs connected both ends of the injury site via directional microfibers, realizing loop growth of the neural network. (Fig. 8B).

3.8. The composite hydrogel scaffold increased the number of matured neurons and promoted axon ingrowth into the lesion site

Mature nerve fibers play an important role in SCI and its repair. During the repair of SCI, nerve cells differentiated from endogenous NSCs migrate along directional fibers, and nerve axons extend to the defect area to connect the two ends of the SCI and restore nerve function [45]. As shown in Fig. 9A, both Tuj1 and MAP2 proteins were expressed in the lesion site implanted with composite hydrogel scaffolds, indicating that neuronal cells derived from migrated endogenous NSCs could differentiate into mature neurons. Axon fibers were expressed less in the lesion site and adjacent areas in the SCI group, which could be attributed to the formation of glial scars after SCI, which blocked axon fiber growth. By contrast, in the Scaffold and WAY-316606 + Scaffold groups, a large number of axon fibers extended into the lesion area. Notably, after quantifying axon length (Fig. 9C), significant differences between the SCI (1.45 ± 0.18 mm), Scaffold (2.83 ± 0.10 mm), and WAY-316606 + Scaffold groups (3.12 ± 0.23 mm) were observed, suggesting that 3D printed composite hydrogel scaffolds can promote axon ingrowth into the lesion area. We also investigated the expression of another mature neuronal marker, NeuN. As shown in Fig. 9B, NeuN and Tuj1 protein distribution were the same as the direction of implantation of the oriented fiber scaffold, which again confirmed that the 3D directional printed microfiber scaffold can guide the growth of nerve cells. The number of NeuN+ cells in the SCI group (18.33 ± 4.37/mm²) was significantly less than that in the Scaffold (39.71 ± 1.63/mm²) and WAY-316606 + Scaffold groups (61.25 ± 5.62/mm²) (P < 0.05, Fig. 9D). Analysis of these data suggested that 3D printed oriented fiber composite hydrogel scaffolds had a positive effect on the regeneration of functional spinal cord tissue. Combined with in vitro cell experiments, 3D printed composite hydrogel scaffolds can activate Wnt/β-catenin signaling to promote neuronal differentiation of NSCs and neuron

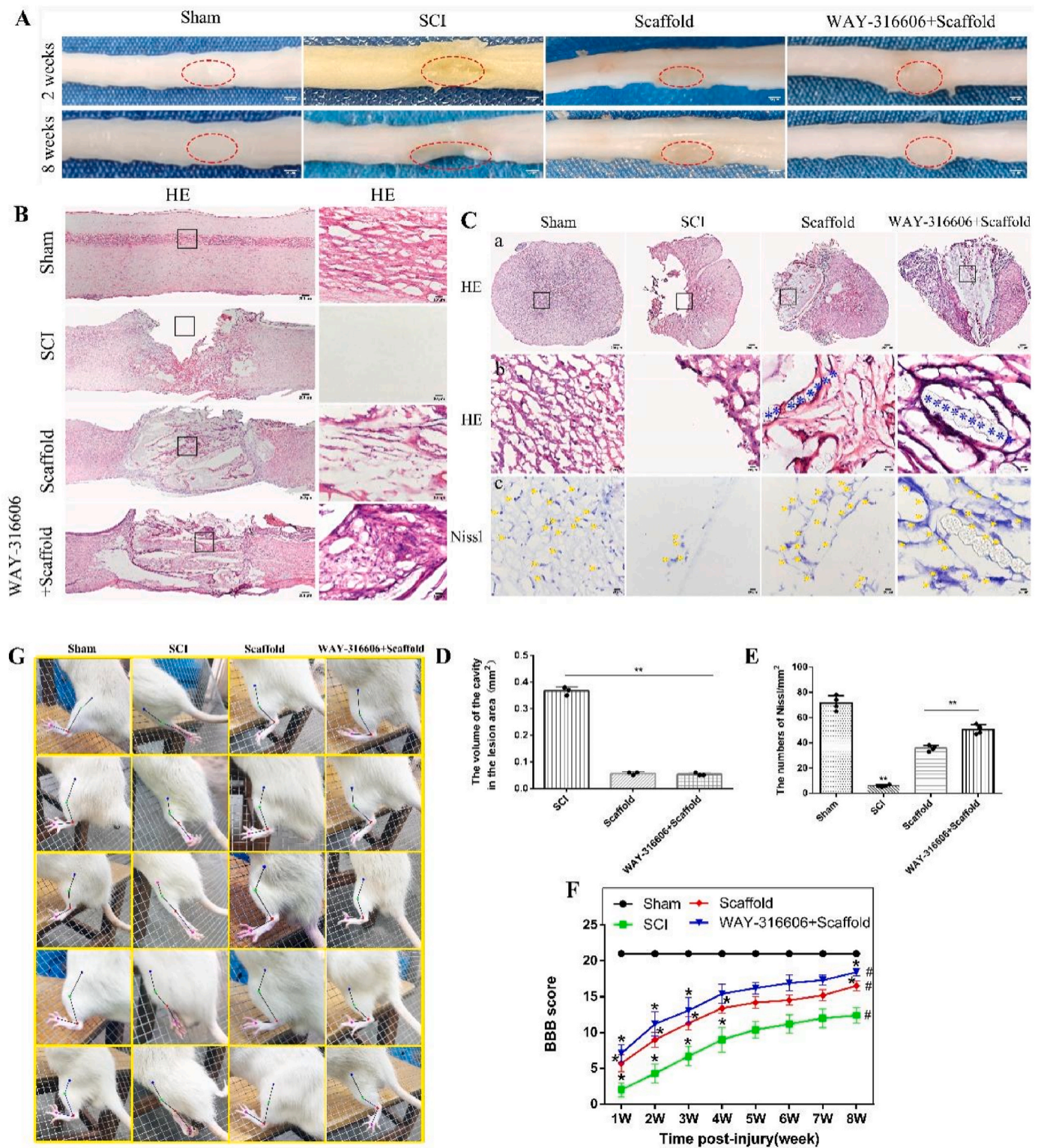X. Zhao et al.

Bioactive Materials 24 (2023) 331–345

339

Fig. 6. Three-dimensionally printed composite hydrogel scaffolds enhanced spinal cord tissue regeneration, reduced diseased cavities, and promoted motor function recovery. A) General view of the spinal cord at 2 and 8 weeks after the operation (scale bar = 50 μm). B) HE staining of a longitudinal section of the spinal cord (large scale on the left = 200 μm, small scale on the right = 20 μm). C) Rows a and b are the HE staining of the transverse section of the spinal cord. Row c is Nissl staining. (a row scale = 200 μm, b and c rows scale = 20 μm. Blue * mark indicates oriented fibers; yellow arrows mark Nissl bodies). D) Cavity area of the lesion area between each group. (**$P < 0.01$, n = 3). E) Statistical plot of the number of Nissl bodies (**$P < 0.01$). F) BBB motor score plot (*$P < 0.05$ within each group; #$P < 0.05$ among groups). G) Grid test. The blue, green, red, and purple dots represent the hip, knee, ankle, and third toes, respectively. The left lower limb was dragged during the upward crawling of the SCI group, while there was no obvious drag in the WAY-316606 + Scaffold and Scaffold groups, and the grip strength of the melon was acceptable.
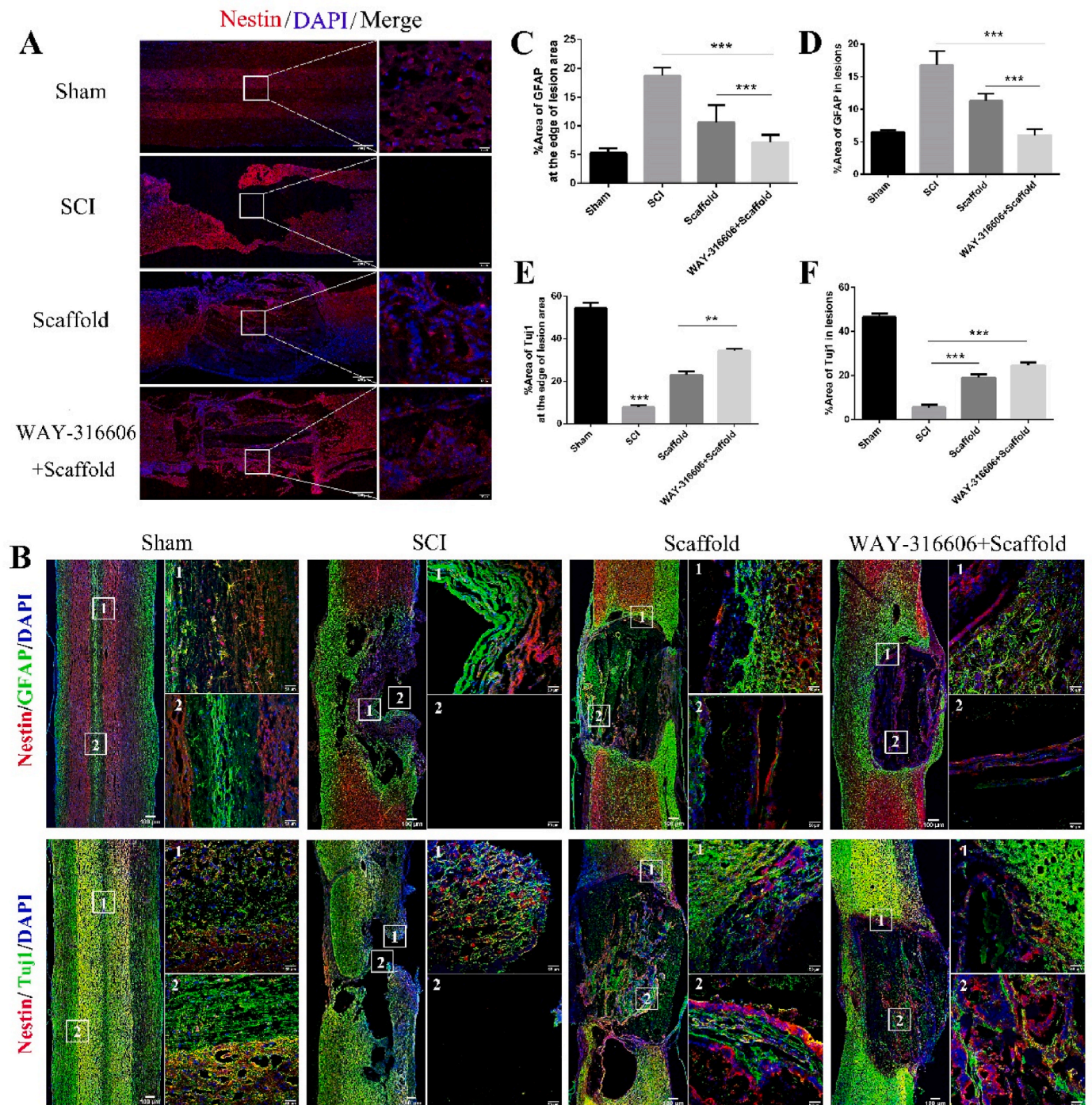
Fig. 7. Three-dimensionally printed composite hydrogel scaffolds can promote endogenous NSC migration and differentiation. A) Immunostaining images of neuronal differentiation of endogenous NSCs at 8 weeks. The number 2.1 in the figure represents the spinal cord lesion area and its adjacent area respectively (scale bar: 100 μm in the large image, 50 μm in the small image; n = 3). B) Immunofluorescence images of endogenous NSCs migrating to the spinal cord lesion. Nestin (red) and DAPI (blue) (scale bar: large image 200 μm, small image 50 μm; n = 3). C, D) Analysis of GFAP expression at the lesion site and adjacent regions, respectively. Error bars represent SD (*P < 0.05, **P < 0.01). E, F) Tuj1 expression was analyzed in the adjacent area and the lesion site, respectively. Error bars represent SD (**P < 0.01, ***P < 0.001, n = 3).

maturation. From this point of view, neural tissue regeneration after SCI can be realized by activating Wnt/β-catenin signaling through the implantation of a 3D printed composite hydrogel scaffold loaded with drugs.

4. Conclusions

In this study, we successfully developed an aligned PCL microfiber bundle-reinforced ASC hydrogel composite hydrogel scaffolds loaded with WAY-316606. The aligned microfiber pattern provided directional topographical guidance for NSCs to migrate and led to a directional neurite extension. Transplanting the drug-loaded composite hydrogel scaffolds into the spinal cord defect effectively filled the SCI defect and achieved spinal cord regeneration through a "bridging" effect. In vitro results showed that the composite hydrogel scaffolds promoted NSC differentiation into neurons while inhibiting their differentiation into
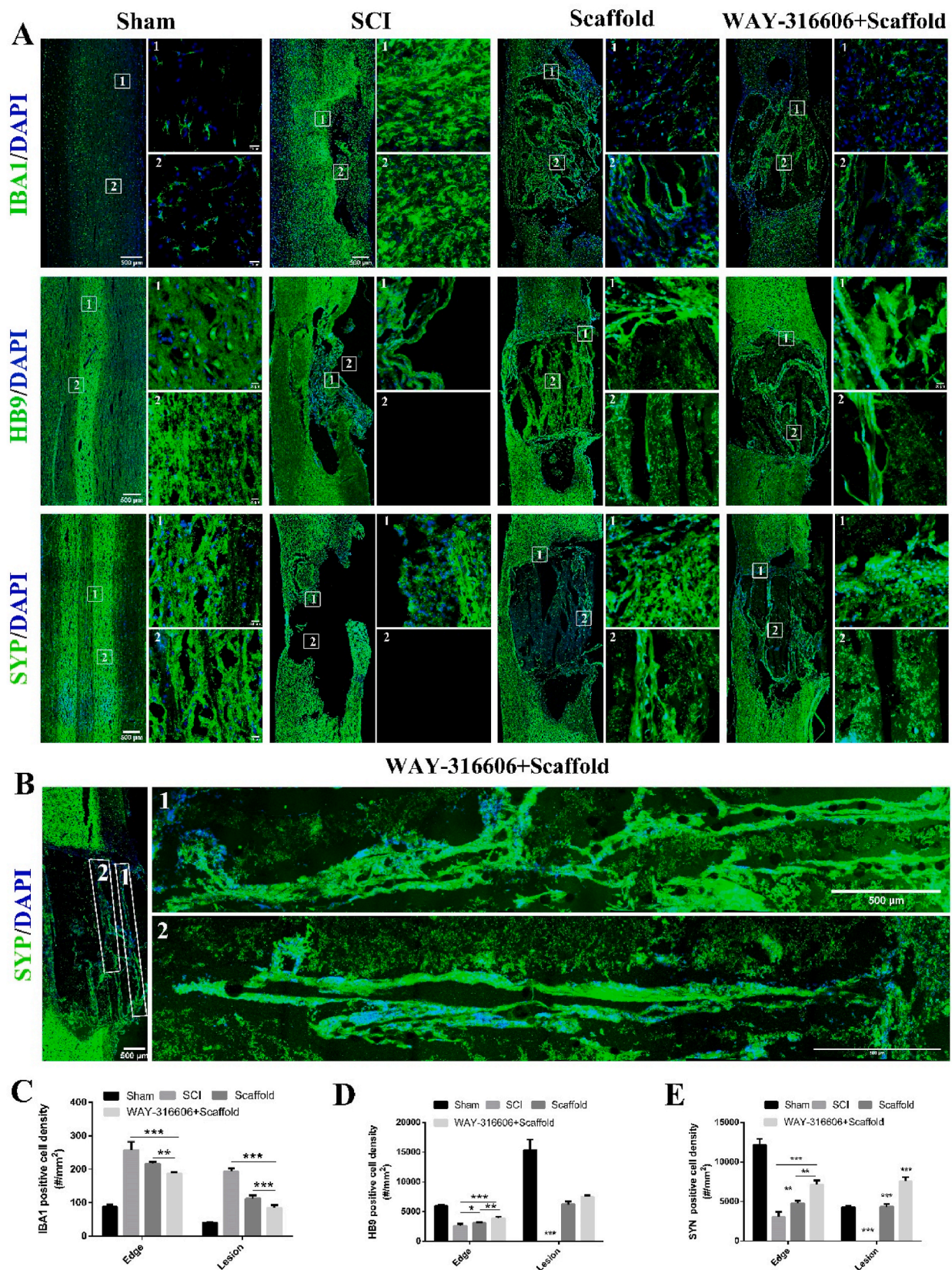
Fig. 8. Inflammation response and motor nerve cell characteristics of regenerated tissue at 2 weeks after SCI. A) Expression of the inflammatory response marker IBA1, the motor neuron marker HB9, and the synaptic marker (SYN). 1 and 2 in the box represent the adjacent area of the SCI and the lesion area, respectively. B) SYN can extend along 3D printed directional microfibers to connect both ends of spinal cord lesions (scale bar = 500 μm). C) Quantification of IBA1^{+} cell density in the spinal cord lesion area and adjacent areas. D) Quantification of HB9^{+} cell density in the spinal cord lesion area and adjacent areas. E) Quantification of SYN[+] cell density in the spinal cord lesion area and adjacent areas. (Error bars indicate SD; **P < 0.01, ***P < 0.001, n = 3).
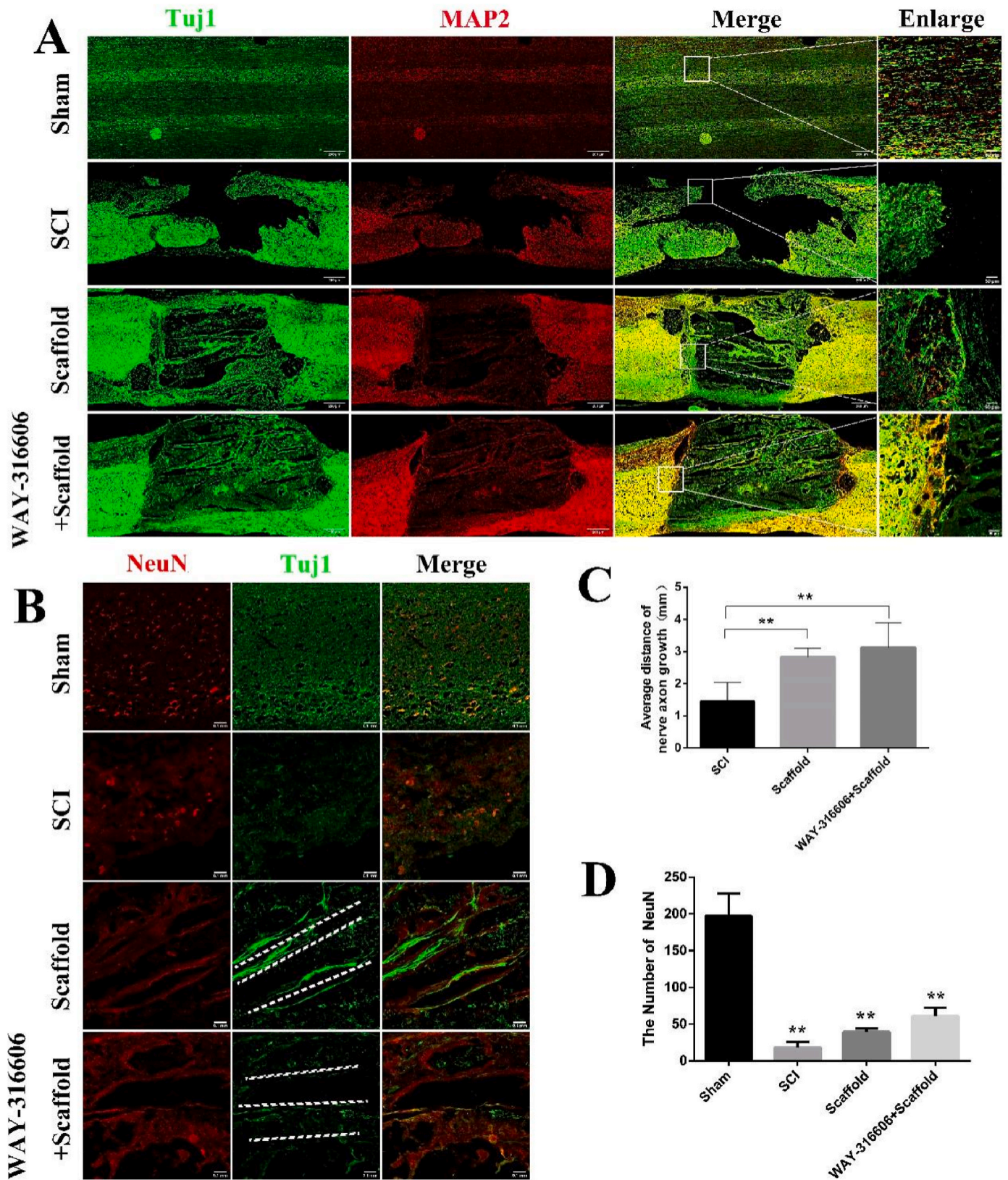
Fig. 9. Three-dimensionally printed composite hydrogel scaffold promoted nerve axon ingrowth into the spinal cord defect and increased the number of neurons. A) Immunofluorescence images of neuronal expression at 8 weeks after surgery. Spinal cords were stained with Tuj1 (green) and MAP2 (red) (Scale bar: large image 200 μm, small image 50 μm, n = 3. B) Immunofluorescence images of NeuN (red) and Tuj1 (green) protein expression. The dashed lines indicate the oriented fiber direction of the 3D printed composite hydrogel scaffolds. (Scale bar = 100 μm n = 3). C) Quantitative analysis of axonal length. Error bars represent SD (**$P < 0.01$, n = 3). D) Quantification of the number of NeuN. Error bars indicate SD (**$P < 0.01$, n = 3).

astrocytes. In vivo study showed that the composite hydrogel scaffolds promoted endogenous NSC migration to the lesion site, oriented the growth of neurites, as did the axial direction of the aligned PCL bundle, inhibited glial scarring, promoted the regeneration of spinal cord tissue, and improved motor function recovery. More importantly, the WAY-316606-loaded composite hydrogel scaffolds activated Wnt/β-catenin signaling to promote NSC differentiation and nerve cell growth, thereby repairing injured spinal cord tissue. This study provides an effective approach to produce desirable drug-loaded composite hydrogel scaffolds with topographical cues to treat SCI.

Ethics statement

All the animal experimental protocols were approved by the Animal Ethics Committee of Youjiang Medical University for Nationalities, and the experimental animals were used according to the requirements of the Animal Welfare Ethics Committee.

CRediT authorship contribution statement

Xingchang Zhao: Conceptualization, Methodology, Formal analysis, Investigation, Writing – original draft. **Xianzhe Lu:** Conceptualization, Methodology, Formal analysis, Investigation, Writing – original draft. **Kai Li:** Conceptualization, Methodology, Formal analysis, Investigation, Writing – original draft. **Shiqiang Song:** Methodology, Formal analysis. **Zhaohui Luo:** Supervision, Writing – review & editing. **Chuanchuan Zheng:** Formal analysis. **Chengliang Yang:** Conceptualization, Supervision. **Xiumei Wang:** Conceptualization, Supervision. **Liqiang Wang:** Writing – review & editing, Supervision. **Yujin Tang:** Supervision, Funding acquisition. **Chong Wang:** Conceptualization, Methodology, Formal analysis, Investigation, Writing – original draft. **Jia Liu:** Resources, Writing – review & editing, Supervision, Funding acquisition.

Declaration of competing interest

The authors declare no competing financial interest.

Acknowledgments

Appendix A. Supplementary data

Supplementary data to this article can be found online at https://doi.org/10.1016/j.bioactmat.2022.12.024.

References

[1] P. Lu, Stem cell transplantation for spinal cord injury repair, Prog. Brain Res. 231 (2017) 1–32, https://doi.org/10.1016/bs.pbr.2016.11.012.
[2] M.E. Vargas, B.A. Barres, Why is Wallerian degeneration in the CNS so slow? Annu. Rev. Neurosci. 30 (2007) 153–179, https://doi.org/10.1146/annurev.neuro.30.051606.094354.
[3] T. Kamradt, C. Rasch, C. Schuld, M. Böttinger, B. Mrle, C. Hensel, C.H. Frstenberg, N. Weidner, R. Rupp, A. Hug, Spinal cord injury: association with axonal peripheral neuropathy in severely paralysed limbs, 1, Eur. J. Neurol. 20 (5) (2013) 843–848, https://doi.org/10.1111/ene.12082.
[4] H. Liu, X. Xu, Y. Tu, K. Chen, L. Song, J. Zhai, S. Chen, L. Rong, L. Zhou, W. Wu, K. F. So, S. Ramakrishna, L. He, Engineering microenvironment for endogenous neural regeneration after spinal cord injury by reassembl ing extracellular matrix, ACS Appl. Mater. Interfaces 12 (15) (2020) 17207–17219, https://doi.org/10.1021/acsami.9b19638.
[5] S. Samantaray, A. Das, D.C. Matzelle, S.P. Yu, L. Wei, A. Varma, S.K. Ray, N. L. Banik, Administration of low dose estrogen attenuates gliosis and protects neurons in acute spinal cord injury in rats, J. Neurochem. 136 (5) (2016) 1064–1073, https://doi.org/10.1111/jnc.13464.
[6] M. Yao, J. Li, J. Zhang, S. Ma, L. Wang, F. Gao, F. Guan, Dual-enzymatically cross-linked gelatin hydrogel enhances neural differentiation of human umbilical cord mesenchymal stem cells and functional recovery in experimental murine spinal cord injury, J Mater Chem B Mater Biol Med 9 (2) (2021) 440–452, https://doi.org/10.1039/D0TB02033H.
[7] J. Liu, J. Chen, B. Liu, C. Yang, D. Xie, X. Zheng, S. Xu, T. Chen, L. Wang, Z. Zhang, X. Bai, D. Jin, Acellular spinal cord scaffold seeded with mesenchymal stem cells promotes long-distance axon regeneration and functional recovery in spinal cord injured rats, J. Neurol. Sci. 325 (1–2) (2013) 127–136, https://doi.org/10.1016/j.jns.2012.11.022.
[8] J. Liu, K. Li, J. Zhou, T. Sun, C. Yang, J. Wei, K. Xie, Q. Luo, Y. Tang, Bisperoxovanadium induces M2-type macrophages and promotes functional recovery after spinal cord injury, Mol. Immunol. 116 (2019) 56–62, https://doi.org/10.1016/j.molimm.2019.09.022.
[9] Kubinová, Biomaterials and magnetic stem cell delivery in the treatment of spinal cord injury, Neurochem. Res. 45 (1) (2020) 171–179, https://doi.org/10.1007/s11064-019-02808-2.
[10] J. Gao, Y. Liao, M. Qiu, W. Shen, Wnt/¦Â-Catenin signaling in neural stem cell homeostasis and neurological diseases, Neuroscientist 27 (1) (2021) 58–72, https://doi.org/10.1177/1073858420914509.
[11] X. Li, C. Fan, Z. Xiao, Y. Zhao, H. Zhang, J. Sun, Y. Zhuang, X. Wu, J. Shi, Y. Chen, J. Dai, A collagen microchannel scaffold carrying paclitaxel-liposomes induces neuronal differentiation of neural stem cells through Wnt/¦Â-catenin signaling for spinal cord injury repair, Biomaterials 183 (2018) 114–127, https://doi.org/10.1016/j.biomaterials.2018.08.037.
[12] G. Chan, D.J. Mooney, New materials for tissue engineering: towards greater control over the biological response, Trends Biotechnol. 26 (7) (2008) 382–392, https://doi.org/10.1016/j.tibtech.2008.03.011.
[13] Y. Rong, W. Liu, Z. Zhou, F. Gong, J. Bai, J. Fan, L. Li, Y. Luo, Z. Zhou, W. Cai, Harpagide inhibits neuronal apoptosis and promotes axonal regeneration after spinal cord injury in rats by activating the Wnt/¦Â-catenin signaling pathway, Brain Res. Bull. 148 (2019) 91–99, https://doi.org/10.1016/j.brainresbull.2019.03.014.
[14] Y. Liu, X. Wang, C.C. Lu, R. Kerman, O. Steward, X.M. Xu, Y. Zou, Repulsive Wnt signaling inhibits axon regeneration after CNS injury, J. Neurosci. 28 (33) (2008) 8376–8382, https://doi.org/10.1523/JNEUROSCI.1939-08.2008.
[15] K. Gao, Z. Shen, Y. Yuan, D. Han, C. Song, Y. Guo, X. Mei, Simvastatin inhibits neural cell apoptosis and promotes locomotor recovery via activation of Wnt/¦Â-catenin signaling pathway after spinal cord injury, J. Neurochem. 138 (1) (2016) 139–149, https://doi.org/10.1111/jnc.13382.
[16] J. Liu, X. Zheng, C. Zhang, C. Zhang, P. Bu, Lcz696 alleviates myocardial fibrosis after myocardial infarction through the sFRP-1/Wnt/beta-Catenin signaling pathway, Front. Pharmacol. 12 (2021), 724147, https://doi.org/10.3389/fphar.2021.724147.
[17] G. Gopinathan, D. Foyle, X. Luan, T.G.H. Diekwisch, The Wnt antagonist SFRP1: a key regulator of periodontal mineral homeostasis, Stem Cell. Dev. 28 (15) (2019) 1004–1014, https://doi.org/10.1089/scd.2019.0124.
[18] Q. Ma, S. Wang, Z. Xie, Y. Shen, B. Zheng, C. Jiang, P. Yuan, C. Yu, L. Li, X. Zhao, J. Chen, A. Qin, X. Fan, Z. Jie, The SFRP1 inhibitor WAY-316606 attenuates osteoclastogenesis through dual modulation of canonical Wnt signaling, J. Bone Miner. Res. 37 (1) (2022) 152–166, https://doi.org/10.1002/jbmr.4435.
[19] Z. Xing, Y. Ni, J. Zhao, X. Ma, Hydrogen peroxide-induced secreted frizzled-related protein 1 gene demethylation contributes to hydrogen peroxide-induced apoptosis in human U251 glioma cells, DNA Cell Biol. 36 (5) (2017) 347–353, https://doi.org/10.1089/dna.2016.3594.
[20] J. Chen, Z. Zhang, J. Liu, R. Zhou, X. Zheng, T. Chen, L. Wang, M. Huang, C. Yang, Z. Li, C. Yang, X. Bai, D. Jin, Acellular spinal cord scaffold seeded with bone marrow stromal cells protects tissue and promotes functional recovery in spinal cord-injured rats, J. Neurosci. Res. 92 (3) (2014) 307–317, https://doi.org/10.1002/jnr.23311.
[21] Q. Feng, K. Wei, S. Lin, Z. Xu, Y. Sun, P. Shi, G. Li, L. Bian, Mechanically resilient, injectable, and bioadhesive supramolecular gelatin hydrogels crosslinked by weak host-guest interactions assist cell infiltration and in situ tissue regeneration, Biomaterials 101 (2016) 217–228, https://doi.org/10.1016/j.biomaterials.2016.05.043.
[22] Z.G. Davis, A.F. Hussain, M.B. Fisher, Processing variables of direct-write, near-field electrospinning impact size and morphology of gelatin fibers, Biomed. Mater. 16 (4) (2021), https://doi.org/10.1088/1748-605X/abf88b.
[23] Q. Chen, X. Mei, Z. Shen, D. Wu, Y. Zhao, L. Wang, X. Chen, G. He, Z. Yu, K. Fang, D. Sun, Direct write micro/nano optical fibers by near-field melt electrospinning, Opt. Lett. 42 (24) (2017) 5106–5109, https://doi.org/10.1364/ol.42.005106.
[24] Y.S. Park, J. Kim, J.M. Oh, S. Park, S. Cho, H. Ko, Y.K. Cho, Near-field electrospinning for three-dimensional stacked nanoarchitectures with high aspect ratios, Nano Lett. 20 (1) (2020) 441–448, https://doi.org/10.1021/acs.nanolett.9b04162.
[25] H. Chen, A. Malheiro, C. van Blitterswijk, C. Mota, P.A. Wieringa, L. Moroni, Direct writing electrospinning of scaffolds with multidimensional fiber architecture for hierarchical tissue engineering, ACS Appl. Mater. Interfaces 9 (44) (2017) 38187–38200, https://doi.org/10.1021/acsami.7b07151.
[26] F.L. He, D.W. Li, J. He, Y.Y. Liu, F. Ahmad, Y.L. Liu, X. Deng, Y.J. Ye, D.C. Yin, A novel layer-structured scaffold with large pore sizes suitable for 3D cell culture prepared by near-field electrospinning, Mater Sci Eng C Mater Biol Appl 86 (2018) 18–27, https://doi.org/10.1016/j.msec.2017.12.016.

[27] Y.K. Fuh, Y.C. Wu, Z.Y. He, Z.M. Huang, W.W. Hu, The control of cell orientation using biodegradable alginate fibers fabricated by near-field electrospinning, Mater Sci Eng C Mater Biol Appl 62 (2016) 879–887, https://doi.org/10.1016/j. msec.2016.02.028.

[28] A. Zimmerling, Z. Yazdanpanah, D.M.L. Cooper, J.D. Johnston, X. Chen, 3D printing PCL/nHA bone scaffolds: exploring the influence of material synthesis techniques, Biomater. Res. 25 (1) (2021) 3, https://doi.org/10.1186/s40824-021-00204-y.

[29] F. Ille, S. Atanasoski, S. Falk, L.M. Ittner, D. Märki, S. Büchmann-Møller, H. Wurdak, U. Suter, M.M. Taketo, L. Sommer, Wnt/BMP signal integration regulates the balance between proliferation and differentiation of neuroep ithelial cells in the dorsal spinal cord, Dev. Biol. 304 (1) (2007) 394–408, https://doi.org/10.1016/j.ydbio.2006.12.045.

[30] A. Seyedsalehi, L. Daneshmandi, M. Barajaa, J. Riordan, C.T. Laurencin, Fabrication and characterization of mechanically competent 3D printed polycaprolactone-reduced graphene oxide scaffolds, Sci. Rep. 10 (1) (2020), 22210, https://doi.org/10.1038/s41598-020-78977-w.

[31] Y.H. Wang, J. Chen, J. Zhou, F. Nong, J.H. Lv, J. Liu, Reduced inflammatory cell recruitment and tissue damage in spinal cord injury by acellular spinal cord scaffold seeded with mesenchymal stem cells, Exp. Ther. Med. 13 (1) (2017) 203–207, https://doi.org/10.3892/etm.2016.3941.

[32] D.X. Ban, Y. Liu, T.W. Cao, S.J. Gao, S.Q. Feng, The preparation of rat's acellular spinal cord scaffold and co-culture with rat's spinal cord neuron in vitro, Spinal Cord 55 (4) (2017) 411–418, https://doi.org/10.1038/sc.2016.144.

[33] B.T. Lang, J.M. Cregg, M.A. DePaul, A.P. Tran, K. Xu, S.M. Dyck, K.M. Madalena, B. P. Brown, Y.L. Weng, S. Li, S. Karimi-Abdolrezaee, S.A. Busch, Y. Shen, J. Silver, Modulation of the proteoglyca,n receptor PTPσ promotes recovery after spinal cord injury, Nature 518 (7539) (2015) 404–408, https://doi.org/10.1038/nature13974.

[34] Y. Luo, L. Fan, C. Liu, H. Wen, S. Wang, P. Guan, D. Chen, C. Ning, L. Zhou, G. Tan, An injectable, self-healing, electroconductive extracellular matrix-based hydrogel for enhancing tissue repair after traumatic spinal cord injury, Bioact. Mater. 7 (2022) 98–111, https://doi.org/10.1016/j.bioactmat.2021.05.039.

[35] L. Li, B. Yan, J. Yang, W. Huang, L. Chen, H. Zeng, Injectable self-healing hydrogel with antimicrobial and antifouling properties, ACS Appl. Mater. Interfaces 9 (11) (2017) 9221–9225, https://doi.org/10.1021/acsami.6b16192.

[36] K. Yamane, T. Mazaki, Y. Shiozaki, A. Yoshida, K. Shinohara, M. Nakamura, Y. Yoshida, D. Zhou, T. Kitajima, M. Tanaka, Y. Ito, T. Ozaki, A. Matsukawa, Collagen-binding hepatocyte growth factor (HGF) alone or with a gelatin-furfurylamine hydrogel enhan ces functional recovery in mice after spinal cord injury, Sci. Rep. 8 (1) (2018) 917, https://doi.org/10.1038/s41598-018-19316-y.

[37] J. Liu, X. Zheng, C. Zhang, C. Zhang, P. Bu, Lcz696 alleviates myocardial fibrosis after myocardial infarction through the sFRP-1/Wnt/¦Â-catenin Si signaling pathway, Front. Pharmacol. 12 (2021), 724147, https://doi.org/10.3389/fphar.2021.724147.

[38] V. Donega, A.T. van der Geest, J.A. Sluijs, R.E. van Dijk, C.C. Wang, O. Basak, R. J. Pasterkamp, E.M. Hol, Single-cell profiling of human subventricular zone progenitors identifies SFRP1 as a target to re-activate progenitors, Nat. Commun. 13 (1) (2022) 1036, https://doi.org/10.1038/s41467-022-28626-9.

[39] N.J. Hawkshaw, J.A. Hardman, I.S. Haslam, A. Shahmalak, A. Gilhar, X. Lim, R. Paus, Identifying novel strategies for treating human hair loss disorders: cyclosporine A suppresses the Wnt inhibitor, SFRP1, in the dermal papilla of human scalp hair follicles, PLoS Biol. 16 (5) (2018), e2003705, https://doi.org/10.1371/journal.pbio.2003705.

[40] S. Xiao, T. Zhao, J. Wang, C. Wang, J. Du, L. Ying, J. Lin, C. Zhang, W. Hu, L. Wang, K. Xu, Gelatin methacrylate (GelMA)-Based hydrogels for cell transplantation: an effective strategy for tissue engineering, Stem Cell Rev Rep 15 (5) (2019) 664–679, https://doi.org/10.1007/s12015-019-09893-4.

[41] A.P. Monteiro, C.M. Rocha, M.F. Oliveira, S.M. Gontijo, R.R. Agudelo, R. D. Sinisterra, M.E. Cortes, Nanofibers containing tetracycline/beta-cyclodextrin: physico-chemical characterization and antimicrobial evaluation, Carbohydr. Polym. 156 (2017) 417–426, https://doi.org/10.1016/j.carbpol.2016.09.059.

[42] F. Berthiaume, T.J. Maguire, M.L. Yarmush, Tissue engineering and regenerative medicine: history, progress, and challenges, Annual review of chemical and biomolecular engineering 2 (2011) 403–430, https://doi.org/10.1146/annurev-chembioeng-061010-114257.

[43] R. Langer, J. Vacanti, Advances in tissue engineering, J. Pediatr. Surg. 51 (1) (2016) 8–12, https://doi.org/10.1016/j.jpedsurg.2015.10.022.

[44] N. Kyritsis, C. Kizil, M. Brand, Neuroinflammation and central nervous system regeneration in vertebrates, Trends Cell Biol. 24 (2) (2014) 128–135, https://doi.org/10.1016/j.tcb.2013.08.004.

[45] T. Fuhrmann, P.N. Anandakumaran, M.S. Shoichet, Combinatorial therapies after spinal cord injury: how can biomaterials help? Adv Healthc Mater 6 (10) (2017) https://doi.org/10.1002/adhm.201601130.